Computer Physics Communications 261 (2021) 107765

Contents lists available at ScienceDirect

Computer Physics Communications

journal homepage: www.elsevier.com/locate/cpc

Open-source modelling of aerosol dynamics and computational fluid dynamics: Nodal method for nucleation, coagulation, and surface growth☆,☆☆

Mino Woo [a,1], Robert T. Nishida [a,b,*], Mario A. Schriefl [c,2], Marc E.J. Stettler [d], Adam M. Boies [a]

[a] Department of Engineering, University of Cambridge, Cambridge, CB2 1PZ, United Kingdom
[b] Department of Mechanical Engineering, University of Alberta, Edmonton, Alberta, T6G 2G8, Canada
[c] Institute of Electrical Measurement and Sensor Systems, Graz University of Technology, Graz 8010, Austria
[d] Centre for Transport Studies, Department of Civil and Environmental Engineering, Imperial College London, London, SW7 2AZ, United Kingdom

ARTICLE INFO

Article history:
Received 8 August 2020
Received in revised form 24 November 2020
Accepted 30 November 2020
Available online 11 December 2020

Keywords:
Aerosol dynamics
Open-source computer code
General dynamic equation
Computational fluid dynamics
Nucleation
Coagulation
Surface growth

ABSTRACT

Understanding formation, growth and transport of aerosols is critical to processes ranging from cloud formation to disease transmission. In this work, a numerical algorithm of aerosol dynamics including nucleation, coagulation, and surface growth was coupled with flow and heat transfer equations enabling the solution of three-dimensional multi-physics aerosol processes in an open-source platform. The general dynamic equation was solved by a nodal method where the particle size distribution was represented by a finite number of nodes. The models were verified by comparing four test cases, (1) pure coagulation, (2) nucleation and coagulation, (3) pure surface growth, and (4) a general dynamic equation that includes the three mechanisms provided in literature. A high temperature aerosol flow in a cooled pipe is chosen as a tutorial case of coupled computational aerosol and fluid dynamics. The aerosolGDEFoam code is available at https://openaerosol.sourceforge.io and can be further modified under GNU general public licence.

Programme summary

Programme title: aerosolGDEFoam
CPC Library link to programme files: https://doi.org/10.17632/3s368jpdx2.1
Developer's repository link: https://openaerosol.sourceforge.io/
Licencing provisions: GNU General Public Licence 3
Programming language: C++
Nature of problem: aerosolGDEFoam solves the general dynamic equation coupled with flow and heat transfer equations enabling the solution of three-dimensional multi-physics aerosol processes using the open-source computational platform, OpenFOAM [1]. The general dynamic equation describes changes in aerosols due to e.g. nucleation, coagulation and evaporation/condensation, processes which depend on local conditions such as temperature and humidity. A zero-dimensional form of the general dynamic equation from Prakash et al. [2] has been implemented and verified with previously published examples.
Solution method: aerosolGDEFoam employs an explicit time-stepping for the time-dependent source terms for aerosol dynamics. The solution methods and schemes provided by OpenFOAM 6 are used for spatial derivatives.
References:
[1] OpenFOAM6, OpenFOAM v6, in The OpenFOAM Foundation, https://openfoam.org/,
[2] Prakash, A., A.P. Bapat, and M.R. Zachariah, A Simple Numerical Algorithm and Software for Solution of Nucleation, Surface Growth, and Coagulation Problems. Aerosol Science and Technology, 2003. 37(11): p. 892–898.

☆ The review of this paper was arranged by Prof. Hazel Andrew.

☆☆ This paper and its associated computer program are available via the Computer Physics Communication homepage on ScienceDirect (http://www.sciencedirect.com/science/journal/00104655).

* Corresponding author at: Department of Engineering, University of Cambridge, Cambridge, CB2 1PZ, United Kingdom.
E-mail address: rn359@cantab.ac.uk (R.T. Nishida).

[1] Present address: National Energy Technology Laboratory, Morgantown, West Virginia 26505, United States.

[2] Present address: AVL DiTEST GmbH, Graz, Austria.

https://doi.org/10.1016/j.cpc.2020.107765
0010-4655/

1. Introduction

Aerosols are any solid and/or liquid particles suspended in a gas (e.g. air) ranging in size from ∼1 nm to 100 μm [1]. Aerosols abound in natural and anthropogenic systems, where dynamics of the aerosol formation and growth dictate a variety of phenomena in areas from health to climate. Aerosol emissions of particulate matter composed of black carbon, primary organic aerosol and secondary organic aerosol [2] are extremely harmful to human health [3,4]. The spread of bacteria and viruses can occur by 'aerosol' and/or 'droplet' transmission where the properties of the pathogen-laden aerosol are highly dynamic during the complex processes of production, transport, and deposition [5]. Understanding of aerosol dynamics and transport can inform interventions for infection control and prevention such as recommendations for masks [6,7], isolation procedures [7], physical distancing, air- and surface-sanitation and ventilation [8] among others [9] such as those applied in response to COVID-19 [10]. Aerosol dynamics influence a variety of fields such as atmospheric air quality [11–13], marine aerosol [14,15], combustion-generated particulates [16–19], and vapour–aerosol dynamics in combustion processes [20,21], where computational aerosol models are increasingly used to model fundamental mechanisms. The increase in computational capabilities enables calculations with high temporal and/or spatial resolutions as well as dynamic particle size distributions, while there still remain issues to trade off computational speed and accuracy depending on the numerical methods [22–24].

Aerosol nucleation, growth, and transport phenomena are highly coupled in an evaporation/condensation system because of the nonlinear dependence of nucleation and particle growth rates on temperature history, concentration gradients, and velocity gradients [25]. Pesthy et al. [26] and Phanse and Pratsinis [27] solved population balance equations for particle nucleation, growth, and coagulation in a simple cylinder and showed that the rate of new particle formation is a strong function of radial and axial positions demonstrating the need for transient, multi-dimensional and multi-phase transport models. Rapid particle growth can occur in high humidity environments whereby growth rates are dictated by particle morphology, size and hygroscopic properties. Volatile aerosols may undergo rapid evaporation during dilution and sampling for experimental diagnostics [28]. The resulting particle size distributions after growth or evaporation determine the transport and likely deposition mechanisms (e.g. in the human lungs). Both numerical and experimental techniques together will advance the understanding of complex and inter-related aerosol dynamics.

Aerosol dynamics including nucleation, coagulation, evaporation, condensation, and electric charging are often described by various forms of the general dynamic equation of aerosols (GDE). A variety of methods to solve the GDE have been reported in literature. Zhang et al. [24] recently provided a systematic review of aerosol dynamics models. Similar to previous reviews, the authors report that a discrete model [29] is most accurate yet computationally expensive as it accounts for every possible particle size. Simplified models such as sectional [30] and discrete-sectional [31] models can sacrifice accuracy and introduce spurious numerical diffusion. The method of moments (MOM), which is based on the solution of differential equations for the moments of the particle-size distribution function [32], is a widely used method in aerosol dynamic simulations coupled with computational fluid dynamics (CFD). This approach has low computational cost due to the relatively small number of transport equations and represents measurable quantities such as total number density. However, MOM requires assumed forms of the aerosol size distribution to close the formulation for lower-order moments. Quadrature method of moments (QMOM) [33] and direct quadrature method of moments (DQMOM) [34] stem from the method of moments and aim to resolve its closure problem. Several studies of CFD-based modal method show this approach is relatively simple and therefore computationally faster than the other methods, while it may cause inaccuracy due to the constraints imposed on the simulated size distribution and standard deviation [22].

As presented in the studies using population balance models, solution of the GDE often benefits from coupling with CFD simulations to account for complex particle behaviours in many practical applications. Though the concept of coupling has existed for more than three decades [35], it is still technically challenging to fully resolve the particle size distribution. Hence, numerical studies with heavy GDE models often use prescribed flow and temperature field [24] or deal only with time evolution of particle size distribution without spatial derivatives [14,36], while CFD simulations often employ simplified methods for solving the GDE [37,38]. Commercial software provides aerosol dynamic models — CHEMKIN-pro has a comprehensive GDE model for size-dependent surface reaction rates [21], and ANSYS Fluent includes a simplified two-equation model for soot formation [39]. Other models have also been studied with the commercial codes via user-defined subroutines [13]. In addition, there are some open-source computer codes available in literature. Prakash et al. [40] proposed a nodal method where the finite-sized sections of the sectional model have been reduced to discrete points called nodes on the size domain. Zhang et al. [24] developed the Aerosol and Air Quality Research Lab-Aerosol Dynamics Model (AAQRL-ADM) that provides four different methods of solving the GDE: discrete, discrete-sectional, MOM, and modal. AeroSolved [41], developed using an open source CFD software OpenFOAM [42], is based on the sectional method and two-moment approach. The OpenFOAM platform has also been used in several studies to incorporate the population balance equation, MOM [43], Extended QMOM (or EQMOM) [44,45], however their focus is mainly the aerosol dynamics in liquid solutions (such as Taylor–Couette flow) or multifluid bubbly flows. Other implementations of conservation equations for aerosols in OpenFOAM are limited to fixed size distributions for exploring e.g. electrical charging [46,47] or lung deposition [48].

The present study aims to verify a well-known basic aerosol dynamics model and implement it into a widely used open-source CFD platform to enable ongoing development of aerosol-CFD models critically needed by the aerosol and CFD communities. By implementing in a CFD platform, readily available momentum, heat and mass transfer models may be directly coupled with aerosol dynamics in three-dimensions necessary for aerosol processes which have significant temperature, concentration or velocity gradients, for example, increasing computational capability allows employing more complicated forms of the GDE in CFD simulations. Hence, a nodal method proposed by Prakash et al. [40] was chosen instead of models based on population balance equations. This approach does not assume a particle size distribution but retains simplicity by using bins of particle volume on logarithmic scale. Thus, the nodal method is computationally inexpensive without sacrificing much accuracy as compared to the sectional method or MOM. Although the discrete nodal structure that simplifies the volume space by discrete numbers of representative volumes inherently introduces errors in the estimation of particle distributions, this intuitive method clearly benefits from its simplicity to be coupled with complex computational fluid dynamic simulations. In the present study, we reviewed the source code for nodal method from Prakash et al. [40] and consolidated those models by replicating the identical example cases in order to verify correct

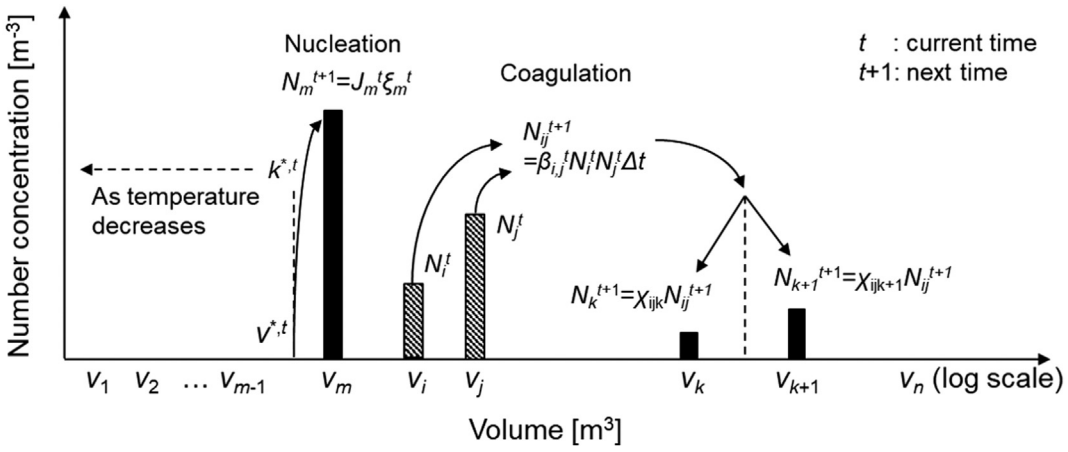

Fig. 1. Schematics of nucleation and coagulation algorithms in nodal method.
Source: Adapted from Prakash et al. [40].

implementation of the equations. The GDE for zero-dimensional time evolution of particle distributions is successfully implemented as source terms of advection/diffusion equations in OpenFOAM enabling computation in complex three-dimensional geometries leveraging a range of readily available momentum, heat and mass transfer solvers. Thus, aerosolGDEFoam (available at https://openaerosol.sourceforge.io) aims to provide an open-source platform where researchers and industrial participants may develop and apply methods to analyse the complex interplay between flows and time evolution of aerosol size distributions. Finally, a tutorial case with detailed description from the problem setup to post-processing is provided to ease the use of the source code.

2. Methodology

The numerical method for the GDE in the present study is based on Prakash et al. [40], which utilises a nodal approach wherein the total volume (or size) range for the aerosol particles is divided into nodes as opposed to discrete sections. The nodal method assigns a unique volume of particle to each node as shown in Fig. 1, and the volume of the monomers, gas molecules which transfer mass to and from the aerosol particles, is selected. The volume of particle for kth node is

$$v_k = v_1 q^k \tag{1}$$

where the subscript 1 represents a monomer which forms particles (clusters) in a supersaturated system according to the classical nucleation theory [49]. v_1 is the volume of monomer and q is the geometric scaling factor defined by

$$q = 10^{\frac{12}{k_{\max}-2}} \tag{2}$$

where k_{max} is the maximum number of nodes.

This model accounts for the particles undergoing nucleation, coagulation and surface growth by evaporation and/or condensation. Fig. 1 schematically explains the nucleation and coagulation algorithm in nodal method. The general dynamic equation of the particle at node k ($k \geq 2$), N_k is

$$\frac{\mathrm{d}N_k}{\mathrm{d}t} = \underbrace{J_k \xi_k}_{\text{nucleation}} + \underbrace{\frac{1}{2}\sum_{\substack{i=2\\ j=2}} \chi_{ijk}\beta_{i,j}N_iN_j - N_k\sum_{i=2}\beta_{i,k}N_i}_{\text{coagulation}} + \underbrace{\begin{cases} \frac{v_1}{v_k - v_{k-1}}\beta_{1,k-1}(N_1 - N_{\mathrm{sat},k-1})N_{k-1} & \text{if } N_1 > N_{\mathrm{sat},k-1} \\ -\frac{v_1}{v_{k+1} - v_k}\beta_{1,k+1}(N_1 - N_{\mathrm{sat},k+1})N_{k+1} & \text{if } N_1 < N_{\mathrm{sat},k+1} \\ -\frac{v_1}{v_{k+1} - v_k}\beta_{1,k}(N_1 - N_{\mathrm{sat},k})N_k & \text{if } N_1 > N_{\mathrm{sat},k} \\ \frac{v_1}{v_k - v_{k-1}}\beta_{1,k}(N_1 - N_{\mathrm{sat},k})N_k & \text{if } N_1 < N_{\mathrm{sat},k} \end{cases}}_{\text{surface growth}} \tag{3}$$

It is noted that when the subscript index k is one, it corresponds to the variables for the monomers. The monomer balance equation which accounts for the monomer concentration changes due to nucleation and surface growth is defined by

$$\frac{\mathrm{d}N_1}{\mathrm{d}t} = J_1\xi_1 + \begin{cases} -\beta_{1,k-1}(N_1 - N_{\mathrm{sat},k-1})N_{k-1} & \text{if } N_1 > N_{\mathrm{sat},k-1} \\ -\beta_{1,k+1}(N_1 - N_{\mathrm{sat},k+1})N_{k+1} & \text{if } N_1 < N_{\mathrm{sat},k+1} \\ -\beta_{1,k}(N_1 - N_{\mathrm{sat},k})N_k & \text{if } N_1 > N_{\mathrm{sat},k} \\ -\beta_{1,k}(N_1 - N_{\mathrm{sat},k})N_k & \text{if } N_1 < N_{\mathrm{sat},k} \end{cases} \tag{4}$$

J_k is the nucleation rate from the self-consistent correction (SCC) model proposed by Girshick et al. [50]

$$J_k = N_{\mathrm{sat}}^2 S v_1 \left(\frac{2\sigma}{\pi m_1}\right)^{0.5} \exp\left(\theta - \frac{4\theta^3}{27\log^2 S}\right) \tag{5}$$

where N_{sat} and S are the saturation concentration of monomer and the saturation ratio defined by

$$N_{\mathrm{sat}} = \frac{p_{\mathrm{sat}}}{k_{\mathrm{B}}T}, \text{ and} \tag{6}$$

$$S = N_1/N_{\mathrm{sat}} \tag{7}$$

where p_{sat} is the saturation pressure. The m_1 in Eq. (5) is the mass of monomer. The dimensionless surface tension and size operator are

$$\theta = \pi\,(6v_1/\pi)^{2/3}\,\sigma/(k_{\mathrm{B}}T), \text{ and} \tag{8}$$

$$\xi_k = \begin{cases} \frac{v^*}{v_k}; & \text{if } v_{k-1} \leq v^* \leq v_k, \\ \frac{v^*}{v_2}; & \text{if } v^* \leq v_1, \\ 0; & \text{otherwise} \end{cases} \tag{9}$$

where v^* is the volume of critical cluster size obtained by the diameter of critical cluster, $d^* = 4\sigma v_1/(k_{\mathrm{B}}T\log S)$. ξ_k represents

the production of particles of critical size (v^*) at the node just larger than k^*.

The coagulation terms $\beta_{i,j}$ represent particle collision frequency in the free molecular regime for particles colliding to form a larger particle [51] ($Kn \equiv \pi\lambda/\left(3v^{1/3}\right) > 10$) is

$$\beta_{i,j} = \left(\frac{3}{4\pi}\right)^{1/6}\left(\frac{6k_BT}{\rho_p}\right)^{1/2}\left(\frac{1}{v_i}+\frac{1}{v_j}\right)^{1/2}\left(v_i^{1/3}+v_j^{1/3}\right)^2. \quad (10)$$

For continuum regime ($Kn \ll 1$) it is defined by Fuchs [52] as

$$\beta_{i,j} = 2\pi(D_i+D_j)(d_i+d_j) \times\left[\frac{d_i+d_j}{d_i+d_j+2(g_i^2+g_j^2)^{1/2}}+\frac{8(D_i+D_j)}{\left(\bar{c}_i^2+\bar{c}_j^2\right)^{1/2}(d_i+d_j)}\right]^{-1} \quad (11)$$

where D_i $\bar{c}_i$ and g_i are the model parameters for particle i as

$$D_i = \frac{k_BT}{3\pi\mu d_i}\frac{5+4Kn_i+6Kn_i^2+18Kn_i^3}{5-Kn_i+(8+\pi)Kn_i^2}, \quad (12)$$

$$\bar{c}_i = \sqrt{\frac{8k_BT}{\pi m_i}}, \quad (13)$$

$$l_i = \frac{8D_i}{\pi\bar{c}_i}, \quad (14)$$

$$g_i = (d_i+l_i)^3 - \frac{(d_i^2+l_i^2)^{1.5}}{3d_il_i} - d_i. \quad (15)$$

Applying conservation of mass at constant density provides a splitting operator χ_{ijk} that allows for the coagulated particles to be proportionally allocated into adjacent bins as seen in Fig. 1 and as defined by

$$\chi_{ijk} = \begin{cases} \dfrac{v_{k+1}-(v_i+v_j)}{v_{k+1}-v_k}; & \text{if } v_k \le v_i+v_j \le v_{k+1}, \\ \dfrac{(v_i+v_j)-v_{k-1}}{v_k-v_{k-1}}; & \text{if } v_{k-1} \le v_i+v_j \le v_k, \\ 0; & \text{otherwise} \end{cases} \quad (16)$$

$N_{sat,k}$ in the surface growth term is the number concentration of monomers over a k-sized particle at saturation as

$$N_{sat,k} = N_{sat}\exp\left(\frac{4\sigma m_k}{RT\rho_p d_k}\right). \quad (17)$$

Further details of the equations presented here may be found in Prakash et al. [40]. The numerical model for the aerosol GDE is implemented into OpenFOAM which is a widely used open source CFD software written in C++. Thus, our implementation of the model enables solving the aerosol behaviour driven by fluid dynamics in three-dimensional complex geometries (necessary for applications with e.g. temperature, concentration or velocity gradients) without assuming the particle size distribution. Previous work by Prakash et al. was similar in concept, but was implemented in zero-dimensional configurations thus limiting their applicability. Moreover, OpenFOAM benefits from its expandability which allows coupling the current model with other essential physics such as chemical reactions and electric charging. OpenFOAM 6 from The OpenFOAM Foundation [42] is chosen as a development platform. Details of the implementation can be found in the supplementary code.

3. Code verification

Implementation of the GDE, Eq. (3), was verified by replicating the example cases exhibited in Prakash et al. [40] which correspond to (1) pure coagulation, (2) nucleation and coagulation, (3) pure surface growth, and (4) GDE including all three phenomena. For verification of pure coagulation, the similarity transformation [53] of predicted self-preserving distribution is compared to those of a discrete-sectional method. The test problem for the other mechanisms is the aluminium particle formation and growth from vapour at 1773 K as it is passed into a condenser with a cooling rate of 1000 K s^{-1}, which is adapted from the work by Panda and Pratsinis [54].

Hence, this is a zero-dimensional problem regarding the time evolutions of monomer and aerosol particles due to nucleation, coagulation, and surface growth. In OpenFOAM, the zero-dimensional problem is modelled by a three-dimensional 1 × 1 × 1 cubic domain with cyclic boundary conditions for all pairs of opposite faces. To cover the size range from 0.3 nm to 3.25 μm, a finite number of nodes spaced linearly on the logarithmic volume scale are specified with a geometric scaling parameter shown in Eq. (2). Except for the pure coagulation example where the dependency of the number of nodes was tested, 40 nodes were used to replicate Prakash et al. [40] for code-to-code verification. The time step of 10^{-5} s is identically used for the example cases in Sections 3, 3.3 and 3.4. In addition, the surface growth model has been revised by correcting the surface growth terms that were not reinitialised at each time step, which resulted in accumulation of unnecessary information.

3.1. Pure coagulation

Swift and Friedlander [55] show that particle size spectra in systems coagulating by Brownian motion reach a self-preserving form independent of the initial distribution after a sufficiently long time. Hence, the implementation of a pure coagulation model was verified by comparing the self-preserving distributions for free-molecular regime of the present study and those from Vemury et al. [56] which employ the discrete-sectional method. Monodisperse particles were initially set to the smallest node ($k = 2$) with the number density of 1×10^{24} m^{-3} according to the C code of Prakash et al. [40]. To compare the results with literature, the particle size distribution was transformed to the dimensionless parameters defined by [53]

$$\eta_k = \frac{v_kN_{tot}}{V_{tot}} \text{ and } \psi_k = \frac{N_kV_{tot}}{\mathrm{d}v_kN_{tot}^2} \quad (18)$$

where the total number concentration and total volume (or volume fraction) are

$$N_{tot} = \sum_{k=2}^{k_{max}-1} N_k \text{ and } V_{tot} = \sum_{k=2}^{k_{max}-1} N_kv_k. \quad (19)$$

Fig. 2(a) presents the predicted self-preserving distribution for free molecular regime with 40, 70 and 100 nodes. The results for 70 and 100 nodes are in very good agreement with the maximum deviation of ψ_k by 7.7% and 3.8% from Vemury et al. [56], respectively. However, the resulting distribution for 40 nodes shows a maximum deviation of 17.3%. This evidence supports the fact that the nodal method with a sufficient number of nodes does not sacrifice much accuracy as compared to the discrete-sectional method despite its simplicity. The self-preserving distribution for the continuum regime, which is not plotted here, is similar to those for free molecular regime shown in Fig. 2 with maximum difference of ψ by 0.45% in this example case with 100 nodes.

The pure coagulation example from the smallest monodisperse particles was particularly sensitive to the time step of calculations. Thus, the total volume of particles in each time step was monitored during the calculation as a verification of mass conservation. The time step was determined to scale with the coagulation characteristic time as

$$\tau = \frac{1}{\beta_{min}N_{tot,min}} \quad (20)$$

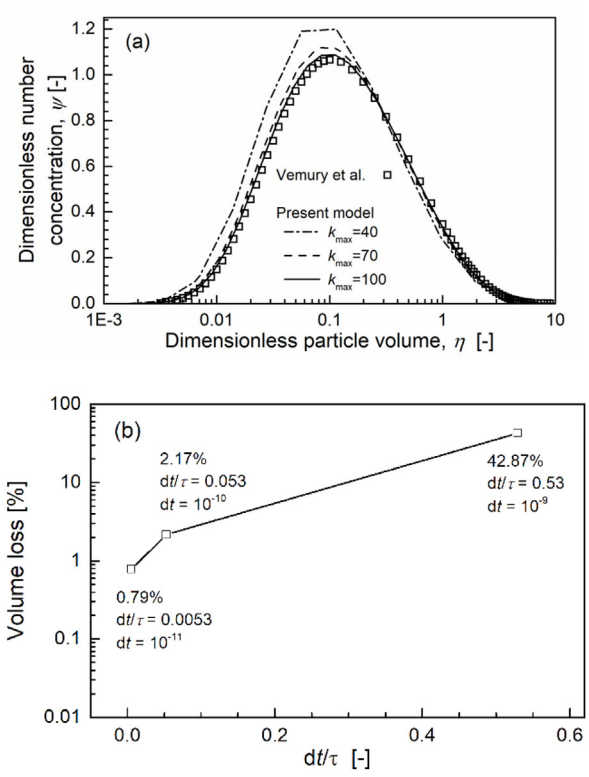

Fig. 2. (a) Self-preserving distribution with different numbers of nodes, (b) volume loss with respect to time step.

where β_{min} is the minimum value of $\beta_{i,j}$ and $N_{tot,min}$ is the minimum value of total number concentration. Fig. 2(b) shows the percent of volume loss from the beginning of calculations using 40 nodes. The volume loss drastically increased as the dt/τ increased from 0.0053 to 0.53. Thus, a time step less than 0.01 of dt/τ is recommended for this particular example, while the C code of Prakash et al. [40] employs the time step criteria as 0.001 of dt/τ. Since the τ increases as the calculation proceeds, the time step for this example varies from 10^{-11} to 10^{-6}.

3.2. Nucleation and coagulation

To initialise nucleation, the saturation ratio S was set to 1.001, and the corresponding monomer concentration was set at the beginning of calculation. Fig. 3 shows the particle size distributions at different times considering only nucleation and coagulation. In this case, the nucleation rate of Eq. (5) and collision frequency of Eq. (10) is employed for coagulation in the free molecular regime. The results of nucleation and coagulation from the present model are in very good agreement with 0.98% maximum deviation of total number concentration ($dN_{tot,max}$) from Prakash et al. [40]. According to Eq. (9), the node where nucleation occurs is determined by the critical cluster size, k^*. Given that the diameter of critical cluster d^* is a function of temperature, it decreases as the system cools down, which causes k^* to shift towards smaller nodes as depicted in Fig. 1. While the particle number concentrations for small particles decrease with time, those for large particles increase due to the coagulation taking place, simultaneously, which therefore results in a bimodal particle size distribution.

3.3. Pure surface growth

Prakash et al. [40] initialise the pure surface growth example by including an initial number concentration of 10^{10} m^{-3} at a monodisperse particle size corresponding to node 25. The initial monomer concentration corresponds to S of 1.001, but the monomer concentration is fixed in this example in order to verify the growth of particles. The same test condition is applied in the present study for comparison. They use three orders of magnitude smaller time step for surface growth model and comment that their code can no longer run for large time steps. However, the present model stabilises this issue with a limiter that always keeps the particle number concentration bigger than a vanishingly small value (10^{-30} m^{-3}). Fig. 4 presents the time evolution of particle size distribution due to the pure surface growth. With the pure surface growth mode, particles either evaporate when the volume of particle is less than v^* or grow otherwise. The initial monodisperse peak broadens as time proceeds with geometric standard deviations progressing from $\sigma_{g,t_0} = 1.02$ to $\sigma_{g,t_3} = 1.43$. Despite using the same time step as for the other models, the results of present study are in good agreement with the $dN_{tot,max}$ of 3.3% from Prakash et al. [40]. This indicates that the present model improves the stability of the rate-determining step, which potentially enhances the overall computation speed.

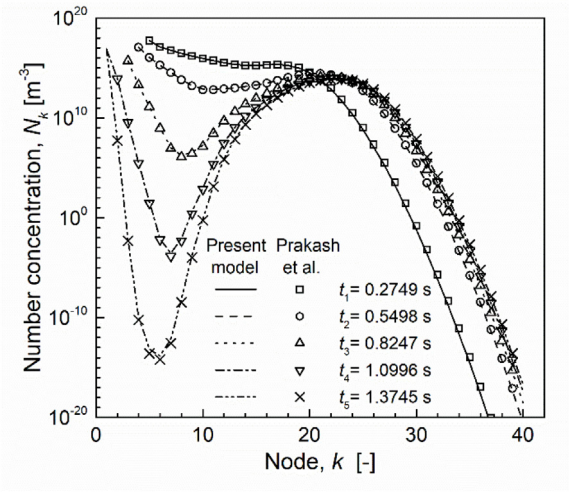

Fig. 3. Time evolution of particle size distribution due to nucleation and coagulation.

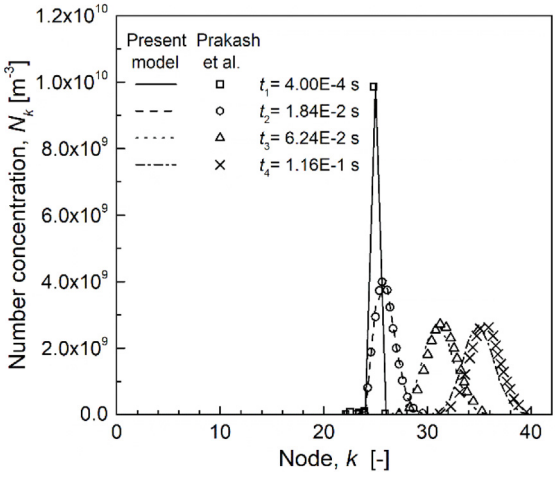

Fig. 4. Time evolution of particle size distribution due to pure surface growth.

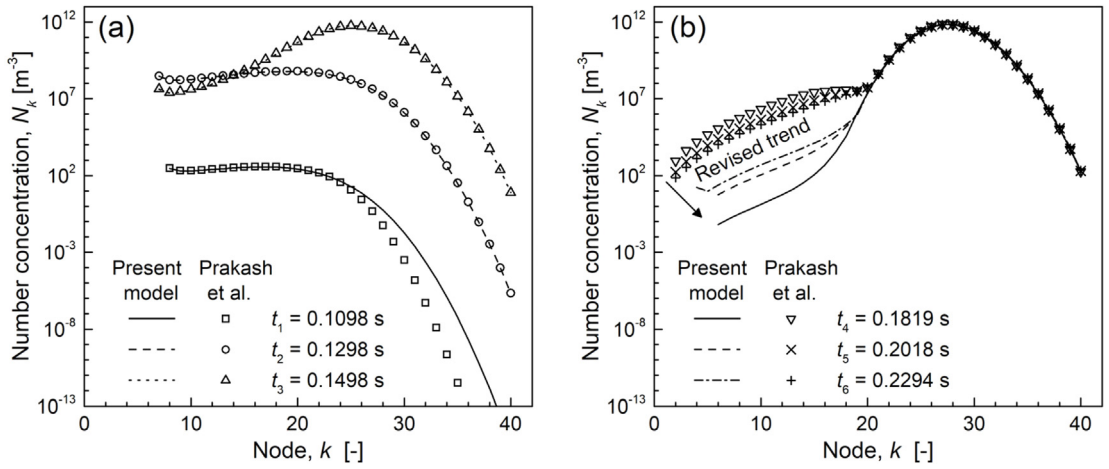

Fig. 5. Time evolution of particle size distribution due to general dynamics including nucleation, coagulation, and surface growth. Revised trend after $t = 0.1498$ s due to the correction of surface growth term from Prakash et al. [40].

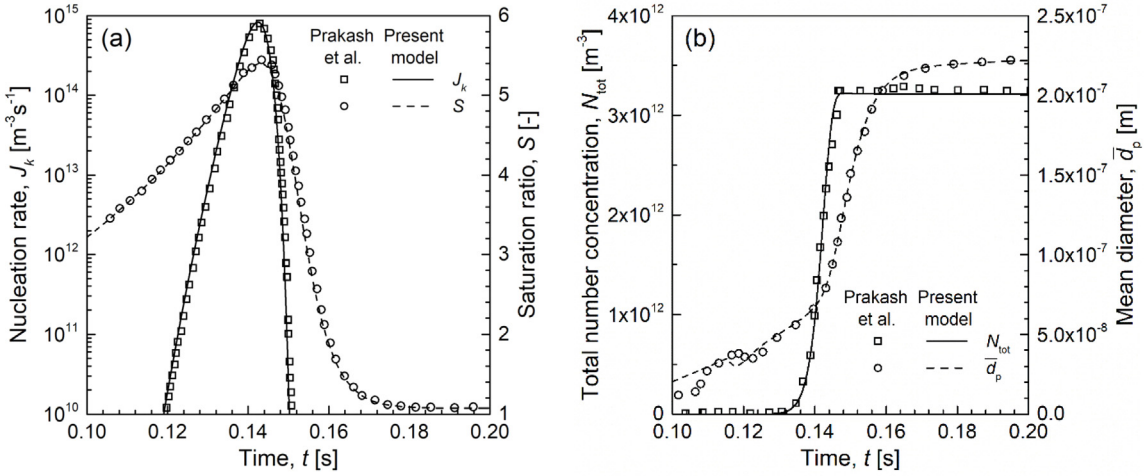

Fig. 6. Comparison of model parameters and respective results of general dynamics example. Time evolution of (a) nucleation rate and saturation ratio, (b) total number concentration and mean diameter.

3.4. General dynamic equation (nucleation, coagulation, and surface growth)

The fourth example is a verification of the GDE that includes all three modes described in Section 2. We utilised the same initial condition as for the nucleation and coagulation example shown in Section 3.2. During code verification, we found it was necessary to update the C code from Prakash et al. to reinitialise the surface growth terms ('addterm' and 'subterm' in the C code) at the beginning of each time step to avoid accumulation of those values from the previous time step. Fig. 5 shows the particle size distributions of the GDE by the present revised model and compares them with Prakash's results [40]. In Fig. 5a, the particle size distributions for the first three time instants where nucleation predominates are in good agreement by 3.8% of $dN_{tot,max}$ and show the trends similar to those of the first example cases shown in Fig. 3. The curve for the first time instant ($t = 0.1098$ s) in Fig. 5a shows deviation gradually increasing with increasing particle size (node). It is presumably caused by the time step (10^{-4} s) in Prakash's code being too large as it disappears with one magnitude smaller time step as for the model in this study. Note that the solutions with the time steps of 10^{-5} and 10^{-6} only differ by 0.3% of $dN_{tot,max}$, which are almost independent of time step.

Meanwhile, the results after $t = 0.1498$ s, where surface growth predominates, deviate and are significantly lower than the Prakash's results as shown in Fig. 5b. The correction primarily affects small particles less than node 21, corresponding to a particle diameter of 35.6 nm. We also confirm that the results from both codes are in good agreement by 1.6% of $dN_{tot,max}$ when implemented with the correction. Thus, our model produces correct size distribution data when modelling aerosol multi-physics, which is in-line with the corrected version of the Prakash's code.

Further model parameters and particle properties from the GDE example are also compared in Fig. 6. Fig. 6(a) displays the nucleation rate and saturation ratio which relate to the nucleation model. Fig. 6(b) shows the total number concentration and mean diameter defined by

$$\bar{d}_p = \left(\frac{6V_{tot}}{\pi N_{tot}}\right)^{1/3} \tag{21}$$

According to the parameters shown in Fig. 6(a), the nucleation rate is highest around $t = 0.14$ s, which results in a drastic increase of the total particle number concentration shown in Fig. 6(b). The particle mean diameter presented in Fig. 6(b) continuously increases after the nucleation peak, which is mainly affected by coagulation and surface growth of the existing particles.

Both Fig. 6(a) and (b) show that the results from the present model and Prakash's study agree very well, although the particle size distributions differ after $t = 0.1498$ s. This evidence, as well as the agreement shown in the previous three test cases, supports the fact that the present model successfully replicated all the example cases in Prakash's study. Consequently, the model is capable of reasonably estimating general particle dynamics and is applicable to more practical simulations by coupling with computational fluid dynamics simulations.

4. Tutorial case

The implementation of the GDE is tested via a tutorial case of a particulate flow in a circular pipe with diameter and length corresponding to 20 cm and 2 m, respectively. To account for the particle movement dictated by flow, the advection term is added to the GDE described in Section 2, while particle diffusion is not considered in this test case. All aerosol dynamics in the GDE (nucleation, coagulation and surface growth) are considered in this example case. The time step is set to 1×10^{-5} s and 40 nodes are employed as done for GDE verification. 'Euler' and 'bounded Gauss linearUpwind limited' numerical schemes were employed for temporal derivative and the advection term, respectively. There are a few steps to execute the tutorial case.

1. Pre-process (mesh generation)
2. Calculation of steady flow and temperature field
3. Calculation of GDE with frozen velocity and temperature

The test procedure and results are explained in the following subsections.

4.1. Pre-process

The circular channel is represented by a two-dimensional axisymmetric computational domain to reduce computation time. The mesh is generated by blockMesh, the default meshing tool in the OpenFOAM software package. Since OpenFOAM only models three-dimensional geometries, the third dimension should also be given to construct the computational mesh. Hence, $200 \times 20 \times 1$ cells for the x, r and angular coordinates are used in this study. Spacing parameters of 5 and 0.1 are used for the x and r directions to specify grid density at the beginning of the channel and near the wall. Left and right sides of the pipe are set to inlet and outlet, and front and back surfaces are set to 'wedge' boundary conditions corresponding to axisymmetric condition in OpenFOAM.

In addition to the mesh generation, velocity, pressure and temperature fields are predetermined using rhoSimpleFoam instead of solved simultaneously with particle transport as there is no feedback from particles to the flow and temperature fields in the present model. A constant velocity of 1 m s^{-1} and temperature of 1500 K are initially specified at the internal field as well as boundary conditions for the channel inlet. Heat loss at the wall is applied as

```
type        externalWallHeatFluxTemperature;
mode        coefficient;
Ta          constant 300.0;
H           uniform 1.5;
kappaMethod fluidThermo;
value       $internalField;
```

Thermophysical parameters for rhoSimpleFoam are taken from air mixture properties in the tutorial of reactingTwoPhaseEulerFoam (/tutorials/multiphase/reactingTwoPhaseEulerFoam/laminar/bubbleColumnEvaporating/constant/thermophysicalProperties. gas). Fig. 7(a) shows the predetermined velocity and temperature fields used for the simulations of particle transport in the next step. Note that the volumetric flux on the cell face denoted as 'phi' is not taken from the results of rhoSimpleFoam because its definition is different depending on compressible and incompressible formulations.

4.2. Problem setup

To start the aerosol dynamic simulation, initialisation of field variables is required. The number of nodes was specified using lookup table named as 'transportProperties' which is placed in './constant'. Particle size can be determined by Eq. (2), composed of the number of nodes and q, due to the node spacing in logarithmic volume space currently hardcoded in the 'createFields' as

```
dimensionedScalar qFactor = Foam::pow(10, 12/(nodes-2));

PtrList<dimensionedScalar> vp(nodes.value());
PtrList<dimensionedScalar> dp(nodes.value());

for (int i=0; i<nodes.value(); i++)
{
    dp.set (i,new dimensionedScalar ("dp",dimensionSet(0,1,0,0,0,0,0),0));
    vp.set (i,new dimensionedScalar ("vp",dimensionSet(0,3,0,0,0,0,0),0));
}
for (int i=0; i<nodes.value(); i++)
{
    if(i==0)
    {
      vp[i] = v1;
    }
    else
    {
      vp[i] = v1 * Foam::pow(qFactor,i);
    }
   dimensionedScalar dpi = Foam::pow(6*vp[i]/pi,1.0/3.0);
   dpi.dimensions().reset(dimensionSet(0, 1, 0, 0, 0, 0, 0));
   dp[i]=dpi;
}
```

Note that the power operation including a certain simple fraction that cannot be represented by finite decimal numbers (e.g. 1/3) does not conserve the units of variables. Hence, units should be reset after those operations to avoid error caused by mismatch of units for further operations.

The number of files for N_k, β and χ depends on the number of nodes given as a part of test condition. Those files are created by a shell script named as 'createFiles' referencing the common files starting with underscore '_' (e.g. _nPartNode) in the './0' directory. Fixed particle number density of 1×10^{10} # m^{-3} is identically set to all nodes for inlet boundary condition by the common file '_nPartNode' corresponding to N_k. The initial number concentration in the entire field is also the same as the inlet value to avoid the potential for numerical instabilities caused by large gradients. Except for inlet and wedge boundaries, a zero gradient boundary condition is employed. Transport properties used for the verification case are identically employed for the tutorial case.

4.3. Results and discussion

The solution reaches steady state after approximately 350,000 iterations corresponding to 3.5 s. Since the current code, incorporating 40 transport equations and writing 1770 parameters, needs heavy computation, the computation time for GDE in two-dimensional axisymmetric domain of 4000 cells is approximately 1 week with a single Intel® Core™ i7-8700 K CPU of 3.70 GHz.

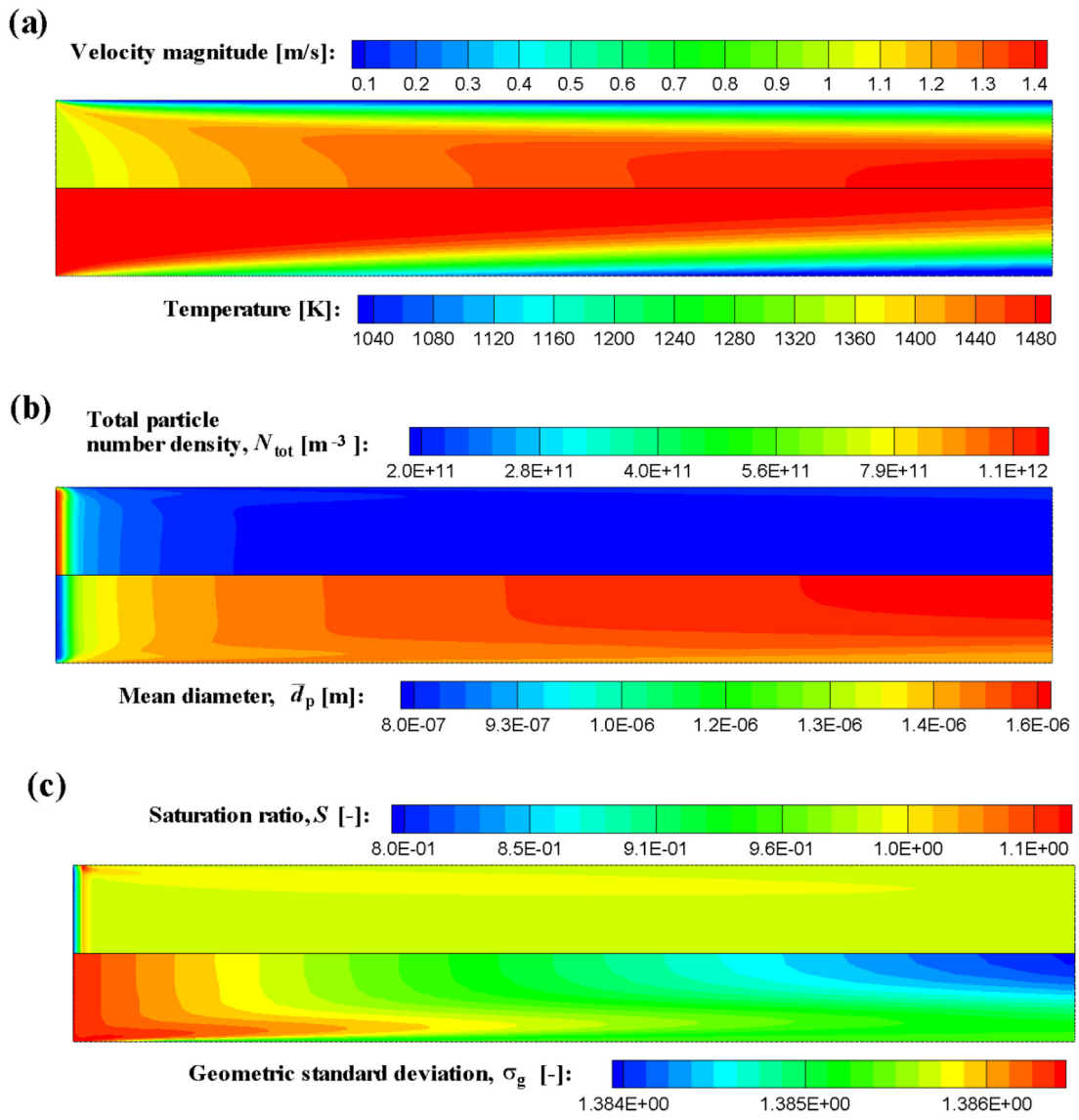

Fig. 7. Results of high temperature aerosol flowing from left (inlet) to right (outlet) in a cooled circular pipe. Distributions of (a) predetermined velocity and temperature, (b) total particle number density and mean diameter, and (c) saturation ratio and geometric standard deviation at steady state.

The results of flow, temperature and particle distributions are exhibited in Fig. 7. Fig. 7(a) presents a typical flow pattern at the beginning of pipe where the uniform velocity given at the inlet is developing to form a radially parabolic velocity profile. Temperature is decreasing due to the heat loss at the pipe wall. Since particle diffusion is not considered, particle movements are solely governed by advection in this case. The distributions of total number concentration and particle mean diameter in Fig. 7(b) which are biased to the pipe core indicate that the advection is properly coupled and drives the particles with the other GDE mechanisms. The total number concentration drastically decreases in the beginning of inlet, while mean diameter increases in contrast. The saturation ratio is almost less than one as shown in Fig. 7(c) and therefore the nucleation rate is zero in the entire domain. Thus, the evolution of particle size in this case is presumably due to the condensation and coagulation. The particle size distribution may slightly change as the geometric standard deviation shown in Fig. 7(d) decreases by approximately 0.002 from inlet to outlet.

Fig. 8(a) shows the particle size distribution along the channel axis depicted by a contour plot. The small particles (node $<$ 20) decrease along the pipe axis, which is mainly dictated by coagulation due to the absence of evaporation. The total number density, total volume and mean diameter are depicted in Fig. 8(b). The figure confirms that the opposite trends of particle total number density and mean diameter are attributed to the almost uniformly-distributed total volume of particle.

The results demonstrate that the GDE is successfully applied in nodal form in a 3D computational fluid dynamics solver enabling investigation of aerosol formation and growth processes where local temperature and flow effects are significant.

5. Conclusions

This study focuses on the development of an open-source computer code for simulations of three-dimensional aerosol flow and general aerosol dynamics including nucleation, coagulation, and surface growth caused by condensation/evaporation. The general dynamic equation of aerosol behaviour is modelled by a nodal approach wherein the particle distribution is simplified by a finite number of nodes as opposed to discrete sections. This method is simpler than the other methods resolving particle size distribution, such as the discrete-sectional method,

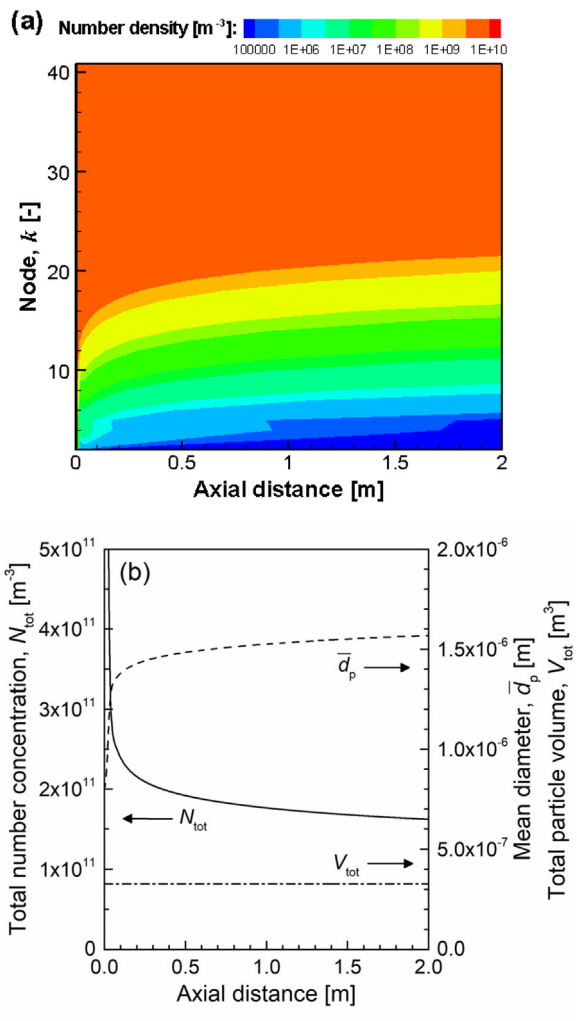

Fig. 8. Particle size distribution (a), total number density, total volume and mean diameter (b) along the axis of the channel.

without sacrificing much accuracy. The numerical algorithm was implemented in the OpenFOAM platform and verified by replicating four test cases in literature, (1) pure coagulation (2) nucleation and coagulation, (3) pure surface growth, and (4) general dynamic equation including the three modes, within 3.8% of maximum deviation of total number concentration. The implemented model is tested by a tutorial case coupled with computational fluid dynamics and shows its capability to be extended for further complex computational aerosol and fluid dynamics simulations.

Nomenclature

d	Particle diameter, m
$\bar{d}_\mathrm{p}$	Particle mean diameter, m
J	Nucleation rate, $\mathrm{m}^{-3}\ \mathrm{s}^{-1}$
k_B	Boltzmann constant, $\mathrm{J\ K}^{-1}$
m	Mass, kg
N	Number concentration, $\#\ \mathrm{m}^{-3}$
R	Gas constant, $\mathrm{J\ mol}^{-1}\ \mathrm{K}^{-1}$
T	Temperature, K
t	Time, s
v	Volume, m^3
q	Geometric scaling factor
Greek symbols	
β	Collision frequency, –
θ	Dimensionless surface tension, –
ξ	Size operator, –
ρ	Density, $\mathrm{kg\ m}^{-3}$
σ	Surface tension, $\mathrm{N\ m}^{-1}$
χ	Size splitting operator, –
Superscripts	
*	Critical
Subscripts	
i, j, k	Node indices
max	Maximum
min	Minimum
p	Particle
sat	Saturation
tot	Total
1	Monomer index

Declaration of competing interest

The authors declare that they have no known competing financial interests or personal relationships that could have appeared to influence the work reported in this paper.

Acknowledgements

This work was supported by Innovate UK (project ref: 103304) and the Natural Sciences and Engineering Research Council of Canada (NSERC) Postdoctoral Fellowships Programme. We also thank Kyungwon Engineering & Communication Inc. (KWEnC) for their technical support on OpenFOAM programming.

References

[1] W.C. Hinds, Aerosol Technology: Properties, Behavior, and Measurement of Airborne Particles, Wiley, 1999.
[2] S.M. Platt, et al., Sci. Rep. 7 (1) (2017) 4926.
[3] L. Künzi, et al., Sci. Rep. 5 (1) (2015) 11801.
[4] A.J. Cohen, et al., Lancet 389 (10082) (2017) 1907–1918.
[5] R.M. Jones, L.M. Brosseau, J. Occup. Environ. Med. 57 (5) (2015) 501–508.
[6] N.H.L. Leung, et al., Nat. Med. 26 (5) (2020) 676–680.
[7] V.C.C. Cheng, et al., Infect. Control Hosp. Epidemiol. 41 (5) (2019) 493–498.
[8] C.J. Roy, D.K. Milton, New Engl. J. Med. 350 (17) (2004) 1710–1712.
[9] J. Fiegel, R. Clarke, D.A. Edwards, Drug Discov. Today 11 (1) (2006) 51–57.
[10] Considerations for wearing cloth face coverings. Centers for disease control and prevention (CDC), 2020, Available from: https://www.cdc.gov/coronavirus/2019-ncov/prevent-getting-sick/cloth-face-cover.html.
[11] C. Pilinis, J.H. Seinfeld, C. Seigneur, Atmos. Environ. (1967) 21 (4) (1987) 943–955.
[12] C.H. Jung, Y.P. Kim, J. Aerosol Sci. 37 (2) (2006) 143–161.
[13] L. Huang, et al., Atmos. Chem. Phys. 14 (23) (2014) 12631–12648.
[14] C. Pilinis, et al., Aerosol Sci. Technol. 32 (5) (2000) 482–502.
[15] F. Gelbard, J.W. Fitzgerald, W.A. Hoppel, J. Geophys. Res.: Atmos. D103 (13) (1998) 16119–16132.
[16] A. Wick, M. Frenklach, H. Pitsch, Combust. Flame 214 (2020) 450–463.
[17] Q. Zhang, et al., Combust. Flame 156 (3) (2009) 697–705.
[18] Q. Zhang, et al., Combust. Theory Model. 12 (4) (2008) 621–641.
[19] T. Kim, Y. Kim, Chem. Eng. Sci. 152 (2016) 426–435.
[20] J.K. Jokiniemi, et al., J. Aerosol Sci. 25 (3) (1994) 429–446.
[21] J.A. Hubbard, M.A. Omana, M.-D. Cheng, J. Therm. Sci. Eng. Appl. 12 (4) (2019).
[22] D. Mitrakos, E. Hinis, C. Housiadas, Aerosol Sci. Technol. 41 (12) (2007) 1076–1088.
[23] J. Pyyk önen, J. Jokiniemi, J. Aerosol Sci. 31 (5) (2000) 531–550.
[24] H. Zhang, et al., Aerosol Sci. Technol. (2020) 1–22.
[25] T.M. Damour, et al., Aerosol Sci. Technol. 39 (5) (2005) 444–451.
[26] A.J. Pesthy, R.C. Flagan, J.H. Seinfeld, J. Colloid Interface Sci. 91 (2) (1983) 525–545.

[27] G.M. Phanse, S.E. Pratsinis, Aerosol Sci. Technol. 11 (2) (1989) 100–119.
[28] V.B. Mikheev, et al., Nicotine Tob Res. 18 (9) (2016) 1895–1902.
[29] F. Gelbard, J.H. Seinfeld, J. Colloid Interface Sci. 68 (2) (1979) 363–382.
[30] F. Gelbard, J.H. Seinfeld, J. Colloid Interface Sci. 78 (2) (1980) 485–501.
[31] W. Jin Jwang, R.C. Flagan, J. Colloid Interface Sci. 123 (2) (1988) 339–352.
[32] M. Frenklach, S.J. Harris, J. Colloid Interface Sci. 118 (1) (1987) 252–261.
[33] R. McGraw, Aerosol Sci. Technol. 27 (2) (1997) 255–265.
[34] D.L. Marchisio, R.O. Fox, J. Aerosol Sci. 36 (1) (2005) 43–73.
[35] F. Stratmann, E.R. Whitby, J. Aerosol Sci. 20 (4) (1989) 437–440.
[36] S.-C. Wang, R.C. Flagan, J.H. Seinfeld, Atmos. Environ. A 26 (3) (1992) 421–434.
[37] J.B. Moss, C.D. Stewart, K.J. Syed, Symp. (Int.) Combust. 22 (1) (1989) 413–423.
[38] M. Fairweather, W.P. Jones, R.P. Lindstedt, Combust. Flame 89 (1) (1992) 45–63.
[39] ANSYS FLUENT Theory Guide, ANSYS, Inc, 2011.
[40] A. Prakash, A.P. Bapat, M.R. Zachariah, Aerosol Sci. Technol. 37 (11) (2003) 892–898.
[41] Computational fluid dynamics code, 2017, http://www.aerosolved.com.
[42] OpenFOAM6, OpenFOAM v6, in The OpenFOAM Foundation, https://openfoam.org/.
[43] J.N.E. Carneiro, V. Kaufmann, W. Polifke, Implementation of a moments model in OpenFOAM for polydispersed multiphase flows, in: Open Source CFD International Conference, Berlin, Germany, 2008.
[44] A. Passalacqua, et al., Chem. Eng. Sci. 176 (2018) 306–318.
[45] E. Askari Mahvelati, P. Proulx, A. Passalacqua, ChemEngineering 2 (2018) 8.
[46] R.T. Nishida, A.M. Boies, S. Hochgreb, J. Appl. Phys. 121 (2) (2017) 023104.
[47] R.T. Nishida, et al., J. Aerosol Sci. 130 (2019) 10–21.
[48] P.G. Koullapis, et al., J. Aerosol Sci. 144 (2020) 105541.
[49] D.R. Warren, J.H. Seinfeld, Aerosol Sci. Technol. 3 (2) (1984) 135–153.
[50] S.L. Girshick, C.P. Chiu, J. Chem. Phys. 93 (2) (1990) 1273–1277.
[51] S.K. Friedlander, Smoke, Dust, and Haze: Fundamentals of Aerosol Dynamics, Oxford University Press, 2000.
[52] N.A. Fuks, The Mechanics of Aerosols, by N.A. Fuchs Translated from the Russian by R.E. Daisley and Marina Fuchs. Translation Edited by C.N. Davies. 1964: Macmillan.
[53] S.K. Friedlander, C.S. Wang, J. Colloid Interface Sci. 22 (2) (1966) 126–132.
[54] S. Panda, S.E. Pratsinis, Nanostruct. Mater. 5 (7) (1995) 755–767.
[55] D.L. Swift, S.K. Friedlander, J. Colloid Sci. 19 (7) (1964) 621–647.
[56] S. Vemury, K.A. Kusters, S.E. Pratsinis, J. Colloid Interface Sci. 165 (1) (1994) 53–59.